Organic Electronics 13 (2012) 2301–2306

Contents lists available at SciVerse ScienceDirect

Organic Electronics

journal homepage: www.elsevier.com/locate/orgel

Non-conventional metallic electrodes for organic field-effect transistors

F. Golmar [a,b,*], M. Gobbi [a], R. Llopis [a], P. Stoliar [a,c,d], F. Casanova [a,e], L.E. Hueso [a,e]

[a] CIC NanoGUNE Consolider, Tolosa Hiribidea 76, 20018 Donostia–San Sebastian, Basque Country, Spain
[b] I.N.T.I. – CONICET, Av. Gral. Paz 5445 Ed. 42, B1650JKA, San Martín, Bs As, Argentina
[c] Laboratoire de Physique des Solides, CNRS UPS, Bât 510, 91405 Orsay, France
[d] ECyT, UNSAM, Martín de Irigoyen 3100, B1650JKA, San Martín, Bs As, Argentina
[e] IKERBASQUE, Basque Foundation for Science, 48011 Bilbao, Basque Country, Spain

ARTICLE INFO

Article history:
Received 13 June 2012
Received in revised form 12 July 2012
Accepted 23 July 2012
Available online 9 August 2012

Keywords:
Organic thin film transistors
Organic field-effect transistors
Non-conventional metallic electrodes
Organic electronics
Fullerene
Pentacene

ABSTRACT

We study micrometer-sized organic field-effect transistors with either Pd or NiFe metallic electrodes. Neither of these materials is commonly used in organic electronics applications, but they could prove to be particularly advantageous in certain niche applications such as organic spintronics. Using organic semiconductors with different carrier transport characteristics as active layer, namely n-type C60 fullerene and p-type Pentacene, we prove that Pd (NiFe) is a very suitable electrode for p- (n-) type semiconductors. In particular, we characterized devices with channel lengths in the order of the micrometer, a distance which has allowed us to evaluate the electronic behavior in a regime where the interfacial problems become predominant and it is possible to reach elevated longitudinal electric fields. Our experimental results agree well with a simple model based on rigid energy levels.

1. Introduction

Organic field-effect transistors (OFETs) have been attracting substantial interest in the last decades due to their optimal operation on multiple (including flexible) substrates, their chemical tunability and their low production costs. OFETs are currently popular in very diverse technological solutions, such as radio frequency identification tags, driving circuits for organic light-emitting diodes (OLEDs), sensors and organic memories [1–8].

OFETs performance, measured for example in terms of their carrier mobility, their ON/OFF ratio or their threshold voltage, has steadily improved thanks to sustained research on two main topics, namely the optimization of organic semiconductors and the development of new dielectric materials for the electric field-effect gate. Organic semiconductor optimization has been pushed forward by synthetic chemistry, via the development of new molecules with more favorable electronic properties and inert behavior in real working environments [9–11], but also by new deposition techniques, creating more controlled and reproducible molecular structures at lower costs [12]. New dielectric materials have allowed a better integration of diverse organic materials in OFETs [13], surpassing the ubiquitous SiO_2 and boosting the performance of some materials by improving growth characteristics and electronic structure at the organic/dielectric interface.

Nevertheless, the organic materials and the gate dielectric are not the only factors controlling the electronic behavior of an OFET. The materials used as electrodes play a very important role in OFET performance, since they are the source of electronic carriers inside the organic channel. However, slightly differently from the research in OLEDs where multiple materials are commonly used, most organic transistors use routinely only Au as electrode. Au has many advantages, probably some of the most important of them being its noble character, its resistance to external chemical aggressions and its capability for further chemical functionalization via diverse self-assembled monolayers. However, Au also has several important

* Corresponding author at: CIC NanoGUNE Consolider, Tolosa Hiribidea 76, 20018 Donostia–San Sebastian, Basque Country, Spain.
E-mail address: fgolmar@nanogune.eu (F. Golmar).

1566-1199/$ - see front matter © 2012 Elsevier B.V. All rights reserved.
http://dx.doi.org/10.1016/j.orgel.2012.07.031

limitations. For example, it adheres poorly to SiO_2 and other insulating materials, requiring an extra adhesion layer (typically either Ti or Cr). It also has a relatively large work function (5.1 eV), limiting the carrier injection into some organic materials if no further functionalization is performed. Last, but not least, it is an expensive metal and its advantageous properties are greatly reduced when alloyed with cheaper elements. Many other conducting materials have been proposed as electrodes for OFETs. Several conventional metals have been tested with diverse success. Other alternatives include transparent conducting materials such as ZnO [14], conducting polymers such as PEDOT:PSS and even carbon structures as carbon nanotubes and graphene [15,16].

In this article, we present experimental results showing that two non-conventional metals, namely Palladium (Pd) and Permalloy ($Ni_{80}Fe_{20}$ or Py) can successfully act as electrodes for either p- or n-type organic semiconductors. Interestingly, both metals could also play a role in the development of organic spintronic devices [17]. Pd is a noble metal and hence very resistant to oxidation and corrosion, while it has a relatively high work function of 5.3 eV [18]. Pd can be alloyed with multiple materials leading for example to interesting ferromagnetic compounds such as the $Pd_{1-x}Ni_x$ series, with potential use in spin-based devices [19]. Also noticeably, it currently markets at roughly half the price of Au.

Py is an alloy with room temperature ferromagnetic behavior. It is widely used in magnetic devices, mainly due to its small coercive field (and hence small electromagnetic losses) and its lack of magnetic crystalline anisotropy. These features make Py ideal for engineering its magnetic properties by shape only. Py is one of the materials of choice for organic spintronic devices [20–23], and it would be very interesting to expand its use to OFETs as well.

Suitably performing micrometer-sized OFETs are fabricated with combinations of either Pd or Py electrodes together with Pentacene (Pc) or Fullerene (C_{60}) as organic materials on top of conventional Si/SiO2 wafers. The electronic behavior of the devices is explained in a first approximation by the interfacial dipolar energy [9,10,24,25] (Δ) between the different metals and organic materials under study. Successful Pd/Pc and Py/C_{60} OFETs were studied in detail, showing the potential of these unconventional metals as carrier injectors for either p- or n-type organic devices.

2. Materials and methods

For this study, we have prepared bottom-gate, bottom-contact OFETs on p^{++}-Si/SiO_2 (150 nm) wafers. The transistor topology consists of interdigitated electrodes with a channel width (W) to channel length (L) ratio (W/L) of 2000, and channel lengths in the range from 0.5 to 2 μm. At these channel lengths, the interfacial properties between the metallic electrodes and the organic semiconductors become dominant in the behavior of the transistors [26,27]. Simultaneously, L above 0.5 μm allows suitably large ratios between the channel width and channel length (W/L). The configuration of our electrodes forces the current path to be well defined, thus avoiding fringe and leakage currents [28,29], while the relatively big currents obtained allow a detailed study of the sub-threshold regime [30]. Also, the L values chosen allow for the study of the channel transport at large longitudinal electric fields (electric field due to the channel bias) [31].

The contact electrodes were patterned on a chip by electron-beam lithography and lift-off. Pd (20 nm) was deposited by sputtering while Py (20 nm) was evaporated. The chips were cleaned with acetone (1 min) and isopropyl alcohol (1 min, ultrasounds) before the organic deposition. The organic materials (either Pc or C_{60}) were evaporated by organomolecular beam deposition (OMBD) in UHV conditions (base pressure $< 1 \times 10^{-9}$ mbar; evaporation pressure $< 1 \times 10^{-8}$ mbar) on top of the chip without primer. The organic material was deposited through a metal shadow mask, avoiding in this way unwanted deposition of material outside the active area of the transistor. Evaporation rates were varied from 0.6 nm/min (Pc) to 1 nm/min (C_{60}). During the organic deposition, the substrates were kept at room temperature. The morphology of the films deposited in the conditions cited just above was checked by atomic force microscopy (AFM; not shown) and it is in accordance with current literature [20,32]. All the device characterization was performed in a high-vacuum probe station in dark conditions. A semiconductor characterization system with two source-measure units (SMU) arranged with sub-femtoampere preamplifier was used for the electrical measurements. One SMU supplied the drain–source voltage (V_{DS}) and recorded the drain–source current (I_{DS}), whereas the second one supplied the gate voltage (V_{GS}) while recording the gate current (I_{GS}). In what follows we do not report I_{GS} values, which were always several orders of magnitude smaller than I_{DS}.

3. Results and discussion

In Fig. 1, we present the transfer characteristics for the four different combinations of metallic electrodes and organic semiconducting channels studied: Pd/Pc, Pd/C_{60}, Py/Pc and Py/C_{60}. The curves are presented up to a V_{DS} value of 10 V and a V_{GS} value of 20 V and are extracted from transistors with 1 μm channel length. We can observe how the combinations Py/C_{60} and Pd/Pc show textbook-like transistor curves, with very high I_{DS} at low V_{DS}, a clear saturation at V_{DS} = 10 V and considerably large values of the I_{DS} when the geometry of the device is taken into account. On the other hand, the combinations Py/Pc and Pd/C_{60} show very poor I_{DS} versus V_{DS} curves, with very weak gate dependence and a total absence of saturation regime up to V_{DS} = 10 V. This is especially clear in the case of the Py/Pc combination, in which there is no recordable I_{DS} up to a $V_{DS} = -3$ V irrespectively of the gate voltage and, in the best case scenario, the maximum output current is three orders of magnitude smaller than in the Py/C_{60} case.

It is also important to note that the C_{60} transistors show n-type behavior, while the Pc ones have a clear p-type character. We can then assume that C_{60} carriers are electrons at the LUMO, while holes at the HOMO are the predominant carriers for Pc [23,33,34].

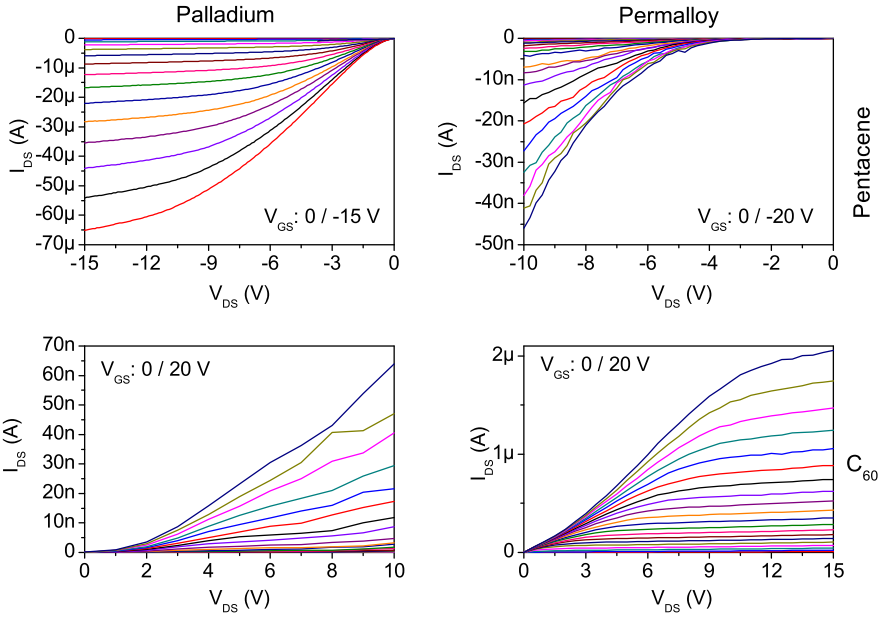

Fig. 1. Drain–source current (I_{DS}) as a function of drain–source voltage (V_{DS}) for four different combinations of metallic electrodes (namely Palladium and Permalloy) and organic semiconductors (Pentacene and C_{60}). V_{DG} increases from 0 to 20 V (−20 V) in step of 1 V for Pc (C_{60}). All the different figures correspond to transistors with 1 μm channel length.

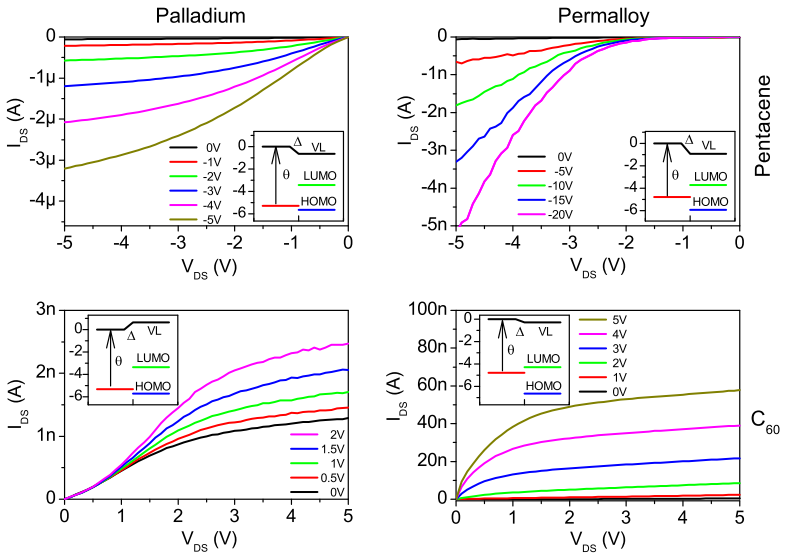

Fig. 2. Drain–source current (I_{DS}) as a function of drain–source voltage (V_{DS}) for four different combinations of metallic electrodes (namely Palladium and Permalloy) and organic semiconductors (Pentacene and C_{60}). Note how the scales are different for the different combinations of materials. All the different figures correspond to transistors with 1 μm channel length. The inset in each figure shows a rigid band-structure energy diagram for the different combinations of materials. θ denotes the work function of the metal electrode and Δ is the shift of the vacuum level (VL) at the interface.

A more detailed view of the current–voltage curves of the same transistors is presented in Fig. 2, focusing on lower V_{DS} values. It is clear again that only the Py/C_{60} and Pd/Pc devices show remarkable transistor behavior, while the other two combinations (Pd/C_{60} and Py/Pc) are not suitable as OFETs. It should also be noted that the transistors whose curves are represented in Fig. 2 have a different L but the same W/L ratio than those of Fig. 1. The measurements presented here are always general and a fair representation of the results obtained from many transistors studied.

Due to the comprehensive study we have developed, fabricating and characterizing four different combinations of materials, we can completely exclude any external factor which might affect the behavior of the transistors such as contamination in the electrodes, problems associated

with the growth of the organic materials and so on. Accordingly, we propose that the different experimental electronic behavior of the OFETs studied here lies preferentially on the band alignment between the metal work function and the highest occupied energy level-lowest unoccupied energy level (HOMO–LUMO) position of the organic semiconductor.

In a first order approximation, when an organic material comes into contact with a metal there is a shift between the vacuum energy levels (VL) of both materials creating an interfacial dipolar barrier (Δ). Accordingly, the injection barrier for the electronic carriers at the metal–organic interface is determined by the energy difference between the metal work function (θ) and the shifted energy level of the closest organic corresponding orbital. This corresponding orbital would typically be the LUMO for n-type organic semiconductors and the HOMO (highest occupied molecular orbital) for the p-type ones.

The work function of Pd and Py are 5.3 eV [18] and 4.9 eV [23] respectively (throughout this paper the energies of the electronic/molecular levels are given with respect to the vacuum level). The relevant conducting orbitals for the organic semiconductors used in this work are the Pc HOMO (5 eV) [9,10] and the C_{60} LUMO (4 eV) [9]. Both the hole-injection and electron-injection barriers (ϕ_h and ϕ_e, respectively) are reported in Table 1. Those values have been calculated considering the formation of interface dipole barriers [10,35].

As can be observed in Table 1, the energy barriers for hole injection into Pc from Pd and for electron injection into C_{60} from Py are relatively small (below 0.5 eV). Conversely, the energy barriers for hole injection into Pc from Py and for electron injection into C_{60} from Pd are much larger (above 1.1 eV). This simple energy level analysis is in agreement with the experimental data presented in Fig. 1 and Fig. 2, where two of the transistors tested worked actually as field-effect devices (Py/C_{60} and Pd/Pc); while the other two combinations of materials (Pd/C_{60} and Py/Pc) yield extremely poor results. Note that we are considering each organic material as purely electron or hole conductor, being this assumption based both on existing literature [23,33,34] and on the recorded experimental behavior of our OFETs.

We selected Pd/Pc and Py/C_{60} transistors for more detailed study. In Fig. 3, we present the transfer curves (I_{DS} versus V_{GS}) for such devices. In both cases the ON/OFF ratio is above six orders of magnitude, reaching even seven orders of magnitude for the Pd/Pc case. This is actually the combination of materials that have a smaller injection barrier for electronic carriers, fact that bundled together with

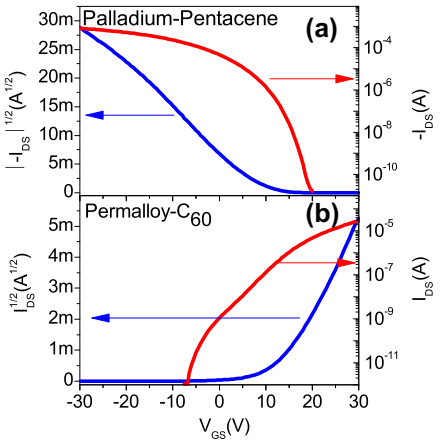

Fig. 3. Transfer curves (I_{DS} versus V_{GS}) for (a) Pd/Pc and (b) Py/C_{60} transistors. The curves have also been plotted as the square root of the drain–source current (left vertical axis).

the better mobility of Pc compared to C_{60}, reinforces our previous interpretation of the I_{DS} versus V_{DS} curves (Figs. 1 and 2) in terms of the metal/organic interfacial energy barrier.

Both the carrier mobility in the linear regime and the subthreshold slope for the different combinations of materials have been extracted, following the definitions presented in Table 2. For the extraction of the field-effect mobility in the linear regime ($\mu_{FET,Lin}$), we determined the slope of the linear regime region of the transfer characteristic (plotted in Fig. 3). The normalized subthreshold slope was extracted as the slope (S) in the transfer characteristic at the onset of the subthreshold region, i.e. for the most positive (negative) V_{GS} value inside the subthreshold region in the p-type (n-type) transistors, and multiplied by the capacitance per unit area of the gate dielectric layer (C_i). Fig. 4 presents the mobility and subthreshold slope values in different conditions.

The values obtained for the mobility are in agreement with the literature for sub-micrometer-size OFETs [28], and there also consistent with expected mobility extrapolated for micrometer-size channel OFETs [36–38]; reaching values close to 0.1 $cm^2/V\,s$ for Pc and 0.01 $cm^2/V\,s$ for C_{60}. These values are quite remarkable, especially taking into account the small dimensions of the transistor studied ($L < 1\ \mu m$ for those specific results) and the deposition of the organic material on plain SiO_2 without the use of any primer. Both the Pd/Pc and Py/C_{60} transistors show a linear relation between the logarithm of the mobility and the square root of the electric field, being the dependence

Table 1
Energy level alignment at the organic semiconductors/metal electrode interface.

Interface (metal/semiconductor)	Electron-injection barrier ϕ_e (eV)	Hole-injection barrier ϕ_h (eV)
Pd/Pc	–	0.34
Pd/C_{60}	1.95	–
Py/Pc	–	1.14
Py/C_{60}	0.49	–

Table 2
Definitions of the different parameters used in the characterization of the organic transistors.

Symbol	Parameter
$\mu_{FET,Lin} = \left\lvert \frac{1}{C_i V_{DS}} \cdot \frac{L}{W} \cdot \frac{dI_D}{dV_{GS}} \right\rvert$	Linear regime field-effect mobility
$S \cdot C_i = \left[\frac{d}{dV_{GS}} log(I_D) \right]^{-1} \cdot C_i$	Normalized subthreshold slope

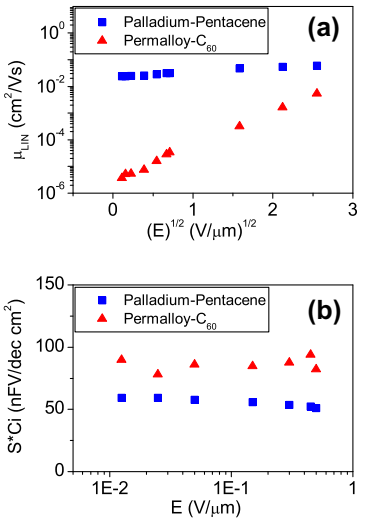

Fig. 4. (a) Dependence of the carrier mobility with the electric field. (b) Dependence of the normalized subthreshold slope with the electric field. Blue square correspond to Pd/Pc data whereas red triangles correspond to Py/C_{60} data. (For interpretation of the references to color in this figure legend, the reader is referred to the web version of this article.)

stronger for the C_{60} case (see Fig. 4a). Such relation between mobility and electric field is known as a Frenkel–Poole equation [31], and arises from simply supposing that charge transport occurs mainly by hopping between localized states. The electric field reduces the hopping barrier between adjacent sites and, if the hopping potential is Coulomb-like, then the hopping probability or mobility have a functional dependence as $\mu = \mu_0\ exp(\beta\sqrt{E}/kT)$; where k is the Boltzmann's constant, T is the temperature, E is the electric field, μ_0 is the mobility at zero field and β is a field-dependent coefficient. The values of β obtained are 1.0 meV/(V/μm)$^{1/2}$ (Pd/Pc) and 7.5 meV/(V/μm)$^{1/2}$ (Py/C_{60}), which are in accordance with those obtained in the literature for similar organic materials [31]. In our specific case, a larger Frenkel–Poole slope for the C_{60} case suggests a larger capability of tuning the intermolecular barriers with the electric field, which is consistent with the mobility being much lower than for the Pentacene case.

The normalized subthreshold slope, which relates the drain–source current with the gate voltage, has values below 100 nFV/dec cm^2. These relatively low values indicate a good coupling between the semiconducting channel and the gate electrode, especially remarkable for a standard 150-nm-thick SiO_2 gate insulator.

4. Conclusion

In this letter, we have fabricated organic field-effect transistors with unconventional metallic electrodes (Palladium and Permalloy) and well-known p- and n-type organic semiconductors (Pentacene and C_{60} fullerene). We have demonstrated that Palladium/Pentacene and Permalloy/C_{60} devices show very satisfactory transistor characteristics, both in the source-drain current and in the transfer curves. In addition, mobility and subtreshold slopes are also comparable to those obtained with conventional metals, such as Au. We argue that the reason behind such favorable behavior is mainly the good matching between the Fermi level of the metal and the corresponding molecular orbitals of the organic semiconductor. The experiments presented here open the way for the use of non-conventional metals for complex application in OFET geometries.

Acknowledgments

This work is supported by the European Union 7th Framework Programme under the European Research Council Grant agreement number 257654 (SPINTROS) and under the NMP project (NMP3-SL-2011-263104-HINTS). This research is also partially funded by the Spanish Ministry of Science and Education under Project No. MAT2009-08494 as well as by the Basque Government Program PI2009-17.

References

[1] A. Dodabalapur, Z. Bao, A. Makhija, J.G. Laquindanum, V.R. Raju, Y. Feng, H.E. Katz, Appl. Phys. Lett. 73 (1998) 142.
[2] P.F. Baude, D.A. Ender, M.A. Haase, T.W. Kelley, D.V. Muyres, S.D. Theiss, Appl. Phys. Lett. 82 (2003) 3964.
[3] B. Crone, A. Dodabalapur, A. Gelperin, L. Torsi, H.E. Katz, A.J. Lovinger, Z. Bao, Appl. Phys. Lett. 78 (2001) 2229.
[4] L. Zhou, A. Wanga, S. Wu, J. Sun, S. Park, T.N. Jackson, Appl. Phys. Lett. 88 (2006) 083502.
[5] K. Baeg, Y. Noh, J. Ghim, S. Kang, H. Lee, D. Kim, Adv. Mater. 18 (2006) 3179–3183.
[6] G. Horowitz, J.Mater. Res. 19 (2004) 1946.
[7] A. Dodabalapur, Mater. Today 9 (2006) 24.
[8] Y. Guo, G. Yu, Y. Liu, Adv. Mater. 22 (2010) 4427.
[9] J. Hwang, A. Wan, A. Kahn, Mater. Sci. Eng. R 64 (2009) 1–31.
[10] A. Kahn, N. Koch, W. Gao, J. Polym. Sci. B: Polym. Phys. 41 (2003) 2529–2548.
[11] H. Klauk, Chem. Soc. Rev. 39 (2010) 2643.
[12] G. Horowitz, Adv. Mater. 10 (1998) 5.
[13] S.Y. Yang, K. Shin, C.E. Park, Adv. Funct. Mater. 15 (2005) 1806–1814.
[14] L. Goris, R. Noriega, M. Donovan, J. Jokisaari, G. Kusinshi, A. Salleo, J. Electron. Mater. 38 (2009) 586.
[15] S. Lee, S. Kang, G. Jo, M. Choe, W. Park, J. Yoon, T. Kwon, Y.H. Kahng, D. Kim, B.H. Lee, T. Lee, Appl. Phys. Lett. 99 (2011) 083306.
[16] R. Schroeder, L.A. Majewski, M. Grell, J. Maunoury, J. Gautrot, P. Hodge, M. Turner, Appl. Phys. Lett. 87 (2005) 113501.
[17] V.A. Dediu, L.E. Hueso, I. Bergenti, C. Taliani, Nat. Mater. 8 (2009) 707.
[18] S.M. Sze, K.K. Ng, Physics of Semiconductor Devices, John Wiley & Sons, 1981.
[19] S. Sahoo, T. Kontos, J. Furer, C. Hoffmann, M. Gräber, A. Cottet, C. Schönenberger, Nat. Phys. 1 (2005) 99.
[20] M. Gobbi, A. Pascual, F. Golmar, R. Llopis, P. Vavassori, F. Casanova, L.E. Hueso, Org. Electron. 13 (2012) 366–372.
[21] M. Michelfeit, G. Schmidt, J. Geurts, L.W. Molenkamp, Phys. Stat. Sol. (a) 205 (3) (2008) 656–663.
[22] W.J.M. Naber, M.F. Craciun, J.H.J. Lemmens, A.H. Arkenbout, T.T.M. Palstra, A.F. Morpurgo, W.G. van der Wiel, Org. Electron. 11 (2010) 743–747.
[23] M. Gobbi, F. Golmar, R. Llopis, F. Casanova, L.E. Hueso, Adv. Mater. 23 (2011) 1609–1613.
[24] A. Molinari, I. Gutiérrez, I.N. Hulea, S. Russo, A.F. Morpurgo, Appl. Phys. Lett. 90 (2007) 212103.
[25] H. Ishii, K. Sugiyama, E. Ito, K. Seki, Adv. Mater. 11 (1999) 605.
[26] P. Stoliar, R. Kshirsagar, M. Massi, P. Annibale, C. Albonetti, D.M. de Leeuw, F. Biscarini, J. Am. Chem. Soc. 129 (2007) 6477.
[27] I. Kymissis, C.D. Dimitrakopoulos, S. Purushothaman, IEEE Trans. Electron. Devices 48 (2011) 1060–1064.
[28] Y. Cao, M.L. Steigerwald, C. Nuckolls, X. Guo, Adv. Mater. 22 (2010) 20.
[29] J.B. Lee, P.C. Chang, J.A. Liddle, V. Subramanian, IEEE Trans. Electron. Devices 52 (2005) 1874.

[30] S. Scheinert, G. Paasch, T. Doll, Synth. Met. 139 (2003) 233–237.
[31] L. Wang, D. Fine, D. Basu, A. Dodabalapur, J. Appl. Phys. 101 (2007) 054515.
[32] H. Yanagisawa, T. Tamaki, M. Nakamura, K. Kudo, Thin Solid Films 464 (2004) 398.
[33] M. Kitamura, Y. Arakawa, J. Phys.: Condens. Matter 20 (2008) 184011.
[34] Y. Yamashita, Sci. Technol. Adv. Mater. 10 (2009) 024313.
[35] U. Zerweck, C. Loppacher, L.M. Eng, Nanotechnology 17 (2006) S107–S111.
[36] H. Klauk, G. Schmid, W. Radlik, W. Weber, L.S. Zhou, C.D. Sheraw, J.A. Nichols, T.N. Jackson, Solid-State Electron. 47 (2003) 297–301.
[37] R. Müller, S. Smout, C. Rolin, J. Genoe, P. Heremans, Org. Electron. 12 (2011) 1227–1235.
[38] N. Takahashi, A. Maeda, K. Uno, E. Shikoh, Y. Yamamoto, H. Hori, Y. Kubozono, A. Fujiwaraa, Appl. Phys. Lett. 90 (2007) 083503.